Control of the Separated Flow behind a Circular Cylinder by Flow Forcing – Experiments and Computations

E. KONSTANTINIDIS[1], C. LIANG[2], G. PAPADAKIS[3], S. BALABANI[3]

[1]*Department of Engineering and Management of Energy Resources, University of Western Macedonia, Bakola & Sialvera, Kozani 50100, Greece. E-mail: ekonstantinidis@uowm.gr*
[2]*Department of Mathematics, University of Glasgow, Glasgow G12 8QW, United Kingdom*
[3]*Department of Mechanical Engineering, King's College London, Strand WC2R 2LS, United Kingdom*

Abstract. This paper describes a complementary experimental and numerical study of the separated flow in the wake of circular cylinder. Wake control is accomplished by superimposing a small-amplitude velocity oscillation on the inflow mean velocity. Predictions from large-eddy simulations are compared against data from particle image velocimetry. The comparisons indicate that the flow physics is well reproduced both qualitatively and quantitatively. It is shown that the timing of vortex shedding imposed by the inflow oscillation controls the phase of the fluctuating fluid force exerted on the cylinder. This relationship, which is analysed in detail, has important implications in selecting control strategies for separated wake flows.

Key words: separated flow, cylinder wake, external forcing, PIV, LES.

1. Introduction

Active and passive control of unsteady separated flows is of great interest from both a fundamental and an engineering point of view. In particular, the wake flow generated by circular cylinders and its control by various means has been the focal point of many research efforts. Much of this effort has concentrated on the practical problem of vortex-excited vibration which involves nonlinear coupling between structural motion and fluid dynamics. Despite the progress achieved in recent years and attested by related reviews on the subject, e.g., see references [10, 11], the understanding of the flow physics is still not complete. Until recently, it has been assumed that enhancement of the wake unsteadiness leads to more intense vortex-induced vibration and therefore the overall aim has been to suppress the unsteadiness. However, recent evidence has suggested that, in fact, the unsteadiness associated with the roll-up of the shear layers and eventual vortex shedding in the wake of cylinders may act as a negative excitation (i.e., damps the vibration) under appropriate conditions. Konstantinidis et al. [5] have shown that a periodic perturbation imposed on the inflow velocity effectively controls the timing of vortex shedding and thereby the phase of the fluid force. In turn, the phase of the fluid force vis-à-vis the motion of an oscillating body determines the energy exchange between the fluid and the body,

or, in other words, determines whether or not self-excited vibrations can occur. It has been argued that this finding explains why the streamwise vortex-induced vibrations of elastically-supported cylinders diminish in the middle of the synchronization region where typically the maximum response amplitude would be expected due to enhancement of the wake unsteadiness [4]. In view of the above, it is important to provide support for this argument and consider in more detail the underlying reasons (flow physics) that produce this paradoxical effect.

In this study, we consider the separated flow behind a circular cylinder under control by external forcing, i.e., by superimposing a periodic oscillation in the inflow velocity as in the original work by Konstantinidis et al [5]. Here, we complement the experiments by large-eddy simulations to attack the problem and derive useful data not available before. One of our goals is to determine the phase of the fluctuating drag force acting on the cylinder in relation to the dynamics of vortex formation. At the same time, comparison between experiments and computations would provide a quantitative assessment of the numerical method employed and its reliability for the study of such unsteady separating flows.

2. Methods of investigation

A complementary experimental and numerical approach is employed to examine the interaction between the wake of a circular cylinder and an inflow with velocity oscillations superimposed upon the mean (forced unsteady flow). The inflow velocity is prescribed by $U(t) = U_m+\Delta U\sin(\omega t)$ where U_m is the inflow mean velocity, ΔU the amplitude of velocity oscillation, and ω the angular frequency of the imposed perturbation. This type of forcing effectively corresponds to the periodic motion of a cylinder prescribed by $x_c(t) = A\cos(\omega t)$ in a steady flow with velocity U_m and $A = \Delta U/\omega$. This transformation will prove useful later to shed light on the vortex-excited oscillation of compliant cylinders as discussed in the Introduction. The Reynolds number for the experiments/computations based on mean velocity and cylinder diameter is 2150/2580. Of primary interest here is the synchronization range that occurs at excitation frequencies (f_e) around twice the natural vortex shedding frequency (f_o) behind a fixed cylinder in unforced flow. The amplitude of velocity oscillations was kept constant at $\Delta U/U_m = 0.05$ for the numerical simulations, i.e., approximately the same as in the experiments.

The experiments were undertaken in a purpose-build water tunnel facility. Results from this experimental programme have appeared in a number of publications where the details of the flow configuration and measurement techniques can be found [4–6]. Some additional, as yet unpublished, data from this study are included in this paper to enable thorough comparisons with the numerical results.

For the computational study, a large-eddy simulation approach is employed with the standard Smagorinsky eddy viscosity model for the unresolved scales

(C_S = 0.1). The incompressible Navier-Stokes equations are low-pass filtered in space and the resulting equations are solved in a fixed frame of reference. A finite-volume method with second order central difference scheme is employed for the spatial discretization on an unstructured collocated grid consisting of 746,688 cells. Note that the computational set-up takes into account the existence of side walls as in the experiment. A second order accurate Crank-Nicholson scheme is employed for time advancement. More details on the numerical scheme and grid independence can be found in Liang and Papadakis [7].

3. Flow statistics

Figure 1 compares the flow statistics between experiment and simulation. The distributions of the streamwise mean velocity, streamwise and cross-stream r.m.s. velocities and the Reynolds shear stress are shown in terms of contour plots employing the same contour levels for both sets of results. We concentrate on a slice of the flow domain perpendicular to the cylinder axis with $0.2 < x/D < 3.2$ and $-1.0 < y/D < 1.0$ in the near wake that is known to play an important role in the vortex formation process and the global wake structure. Overall, the distributions of all the flow statistics are remarkably similar between experiment and simulation. There is also very good agreement on the demarcation of the wake bubble. For example, the length of the recirculation bubble, marked by the location of zero streamwise mean velocity on the wake centreline, is $L_b/D = 1.12$ from both the experiment and simulation (cf. to the value 2.06 in steady flow [4]). Similar observations can be made for the locations where the maxima in the streamwise and cross-stream r.m.s. velocities occur.

The r.m.s. velocities are slightly over-predicted from the simulation compared with the experiment and so is the Reynolds shear stress (Figure 1b, c, d). It is difficult to pinpoint the exact reason for this difference. It might be attributed to grid resolution, subgrid-scale model or the size of the computational domain. For example, the spanwise length of the cylinder is equal to $10D$ in the experiment (cylinder terminates at the test section walls) compared to πD in the simulation (periodic boundary condition at ends). Spanwise resolution DNS studies at Re = 3900 indicate a relatively weak effect of the spanwise length on the computed quantities [3]. Hence, the spanwise length might not be too critical. Another factor is the exact value of the frequency ratio f_e/f_o. It has been found that this ratio has a strong effect on the intensity of wake fluctuations [4]. Therefore, even a small mismatch of the f_e/f_o ratio can result in rather large differences in r.m.s. velocities. Note that the natural shedding frequency is subject to uncertainty, particularly for the computations due to the short number of cycles resolved. Therefore, precise comparisons should be made with caution.

Both the experiment and the simulation indicate high levels of the Reynolds shear stress near the base of the cylinder, in line with the shortening of the wake bubble noted above. This contrasts with the wake behaviour in unforced flow

which is typically characterized by inactive flow in the base region at low subcritical Reynolds numbers ($\mathrm{Re} \approx 2000$). A similar intensification of flow activity in the base region is observed when the Reynolds number is increased from 10^3 to 10^4 as it has been noted in a number of previous studies [3, 4, 8]. This behaviour has been attributed to the upstream movement of the transition point along the separating shear layer with increasing Reynolds number. However, whether the same remark holds true due to flow forcing is debatable. This might be expected if the excitation frequency were close to the shear layer frequency. According to the empirical correlation proposed by Prasad and Williamson [9] the shear layer frequency is about ten times the unforced vortex shedding frequency around $\mathrm{Re} \approx 2000$ and, hence, the excitation frequency is one fifth of the shear layer frequency. Thus, it seems unlikely that the inflow excitation can interact with shear layer transition per se for such remote frequencies.

4. Wake three-dimensionality

Figure 2(a) shows a three-dimensional view of the instantaneous spanwise vorticity distribution $\omega_z D/U_m$ in the wake. Positive and negative vorticity isosurfaces are coded red and blue, respectively. The roll-up of the separating shear layers above and below the cylinder and the formation of the primary spanwise vortices is illustrated clearly. The vortex filaments are parallel to the cylinder axis and spanwise undulations develop upon separation. These undulations give rise to the generation of streamwise vorticity as shown in Figure 2(b); the same three-dimensional view as in Figure 2(a) but showing the instantaneous streamwise vorticity distribution $\omega_x D/U_m$. The generation of streamwise vorticity is consistent with 'mode-B instability' developing in cylinder wakes at Reynolds numbers greater than 280 approximately [2, 12]. A feature that is not evident in the motionless pictures is the temporal variation of the locations along the cylinder span where the undulations develop. An animation of the cross-stream velocity component in the plane parallel to the cylinder axis and passing through it (not included here) exhibits characteristic spatio-temporal deviations in the sign of the velocity fluctuations associated with the generation of streamwise vorticity. In this animation, it is observed that the locations where streamwise vortices emanate wander randomly along the cylinder span. Therefore, the streamwise vortices can only be linked to individual primary vortices.

Figure 3(a) shows the vorticity distribution in two perpendicular planes in the wake (the components of normalized vorticity normal to each plane are shown, i.e., $\omega_z D/U_m$ and $\omega_y D/U_m$). From this representation it can be inferred that the streamwise vortices develop in the braid regions between primary vortices; the $\omega_y D/U_m$ component is appreciable only in these regions. The streamwise vortices exhibit considerable deviations in its spatio-temporal evolution from one cycle to the next. The wavelength of the spanwise undulations is not constant, being less

than one diameter, on average. This can also be inferred by the cross-correlation of the velocity fluctuations along the cylinder span, another measure of the wake three-dimensionality, shown in Figure 3(b). The cross-correlation of the streamwise velocity fluctuations R_{uu} drops gradually to 0.6 for a separation of $0.4D$. For wider separations, R_{uu} remains constant because the primary vortices are correlated along the entire span. There is good agreement between the experimental and computational results for similar conditions.

5. Timing of vortex shedding

Figure 4 shows snapshots of the instantaneous vorticity distribution in the wake. Exactly the same procedure was employed to compute vorticity distributions from both experimental and numerical data in order to minimize associated effects. The snapshots correspond approximately to the same phase near the minimum inflow velocity as shown in the accompanying subfigures. The similarity of the vorticity distributions is striking; both snapshots display the shedding of positive vorticity from the lower side of the cylinder as the entrainment of the shear layer from the upper side has cut-off the supply of vorticity into the shed vortex. The flapping motion of the shear layer causes cross-annihilation of oppositely signed vorticity in the near wake. Downstream of the vortex formation region, the vorticity shed during previous cycles reorganizes into an array of vortex structures resembling the Bernhard–von Kármán vortex street. However, the shed vorticity is broken up into pieces by the action of turbulent mixing. There is a good agreement between experiment and simulation on the length scales produced in the wake.

Another point of agreement between experiment and simulation is the occurrence of a 2P-like vortex mode involving the splitting of vorticity into pairs above and below the wake centreline. This issue has been addressed in detail previously with reference to the experiments where bimodal behaviour was observed [4]. A similar behaviour was observed from the computational study, more clearly illustrated in animations of the vorticity distribution (not included).

The comparison in Figure 4 suggests that the timing of vortex shedding is correctly predicted by the simulation. To take this point a step further, we tracked the flow oscillation across the wake axis at the location where the transverse r.m.s. velocity v' becomes highest from LES data (x/D = 1.45). The data were phase-averaged in order to eliminate cycle-to-cycle variations and the result is shown in Figure 5(a). The maximum of the cross-flow oscillation occurs near the middle of the inflow deceleration phase. This instant corresponds to the beginning of the downstream stroke for the equivalent case of a cylinder oscillating in a time-steady flow. This is in agreement with the experimental findings; for forcing frequencies below half the unforced shedding frequency, the timing of the maximum cross-flow oscillation and, hence, the timing of vortex shedding is shifted towards the beginning of the downstream stroke [5].

6. Vortex-induced forces

Figure 5(b) shows the variation of the drag coefficient as a function of time and the inflow velocity by means of a 3-D trajectory. The drag coefficient oscillates about a mean value with a frequency controlled by flow forcing, forming a limit cycle in the U–C_d plane. The drag coefficient becomes maximum in the middle of the acceleration phase of the inflow oscillation in every cycle. Clearly, this variation indicates the nonlinear interaction between flow forcing and wake response; if the response was linear then the drag coefficient would be maximum at the peak inflow velocity. The peak (trough) value of the drag coefficient exhibits considerable cycle-to-cycle variations, a feature that illustrates the turbulent character of the wake. The mean value of the drag coefficient increases relative to that in unforced flow by a factor of 1.23 in good agreement to previous experimental studies [1].

The phase ϕ of the drag force $C_d(t)$ relative to the displacement $x_c(t)$ for the equivalent case of a cylinder oscillating in steady flow was estimated using cross-spectral analysis. Both time-resolved and phase-averaged data provided the same result $\phi = 1.3°$ for $f_e/f_o = 1.88$. As a consequence, the energy transfer from the fluid to the cylinder over an average cycle $E = \int_T C'_d(t)\mathrm{d}x_c$, is negligible. This finding supports the hypothesis that the timing of vortex shedding imposes a fluctuating drag force in-phase with displacement and unambiguously explains the lack of vortex-excited vibrations near the middle of the synchronization range. Further computations for a forcing frequency $f_e/f_o = 2.09$ show that the phase becomes negative ($\phi = -26.6°$) indicating that energy is transferred from an oscillating cylinder to the fluid, i.e., the fluctuating drag force acts as a negative excitation. Extrapolating from this result, it might be expected that the phase of the drag force becomes positive for $f_e/f_o < 1.88$. More computations are in progress in order to resolve the phase of the drag force throughout the synchronization range.

7. Conclusions

This paper describes a combined experimental and numerical study of the separated flow behind a circular cylinder controlled by small-amplitude inflow velocity oscillations. Comparison of the results indicates that many characteristics of the physical experiment are predicted correctly by the large-eddy simulations; these include the flow statistics in the separated region, the patterns of vorticity distribution in the wake, the spanwise correlation of velocity fluctuations in the shear layers and the timing of vortex shedding relative to the inflow oscillation. Furthermore, the simulation has provided information on the three-dimensional structure of the wake, for example the generation of streamwise vortices, as well as the magnitude and phase of the vortex-excited forces exerted on the cylinder. One of the most important findings is that the

timing of vortex shedding at the middle of the deceleration phase induces a fluctuating drag force out-of-phase with inflow oscillation, or in-phase with cylinder displacement for the equivalent case of streamwise cylinder oscillations in steady flow. This finding has important implications in selecting control strategies for separated wake flows, e.g., to enhance transport rates and/or repress vortex-excited vibrations.

References

1. Armstrong, B.J., Barnes, F.H. and Grant, I., A comparison of the structure of the wake behind a circular cylinder in steady flow with that in a perturbed flow. *Phys. Fluids* **30** (1987) 19–26.
2. Brede, M., Eckelmann, H. and Rockwell, D., On secondary vortices in the cylinder wake. *Phys. Fluids* **8** (1996) 2117–2124.
3. Dong, S., Karniadakis, G. E., Ekmekci, A. and Rockwell, D., A combined direct numerical simulation-particle image velocimetry study of the turbulent near wake. *J. Fluid Mech.* **569** (2006) 185–207.
4. Konstantinidis, E., Balabani, S. and Yianneskis, M., The effect of flow perturbations on the near wake characteristics of a circular cylinder. *J. Fluids Struct.* **18** (2003), 367–386.
5. Konstantinidis, E., Balabani, S. and Yianneskis, M., The timing of vortex shedding in a cylinder wake imposed by periodic inflow perturbations. *J. Fluid Mech.* **543** (2005) 45–55.
6. Konstantinidis, E., Balabani, S. and Yianneskis, M., Bimodal vortex shedding in a perturbed cylinder wake, *Phys. Fluids* **17** (2007) 011701.
7. Liang, C. and Papadakis, G., Large eddy simulation of pulsating flow over a circular cylinder at subcritical Reynolds number, *Comp. Fluids* **36** (2007) 299–312.
8. Lin, J. C., Towfighi, J. and Rockwell, D., Instantaneous Structure of the near-Wake of a Circular-Cylinder - on the Effect of Reynolds-Number. *J. Fluids Struct.* **9** (1995) 409–418.
9. Prasad, A. and Williamson, C. H. K., The instability of the shear layer separating from a bluff body. *J. Fluid Mech.* **333** (1997) 375–402.
10. Sarpakaya, T., A critical review of the intrinsic nature of vortex-induced vibrations. *J. Fluid Struct.* **19** (2004) 389–447.
11. Williamson, C.H.K. and Govardhan, R., Vortex-induced vibrations. *Annu. Review Fluid Mech.* **36** (2004) 413–455.
12. Wu, J., Sheridan, J., Hourigan, K. and Soria, J., Shear layer vortices and longitudinal vortices in the near wake of a circular cylinder. *Exp. Thermal Fluid Sci.* **12** (1996) 169–174.

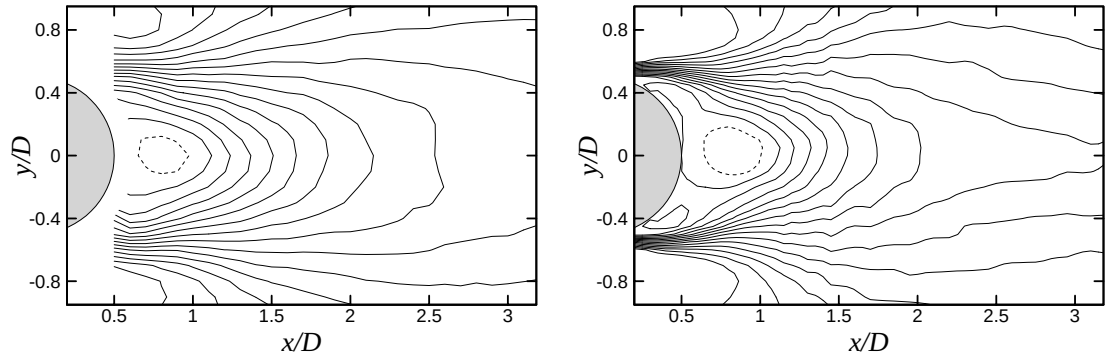

(a)

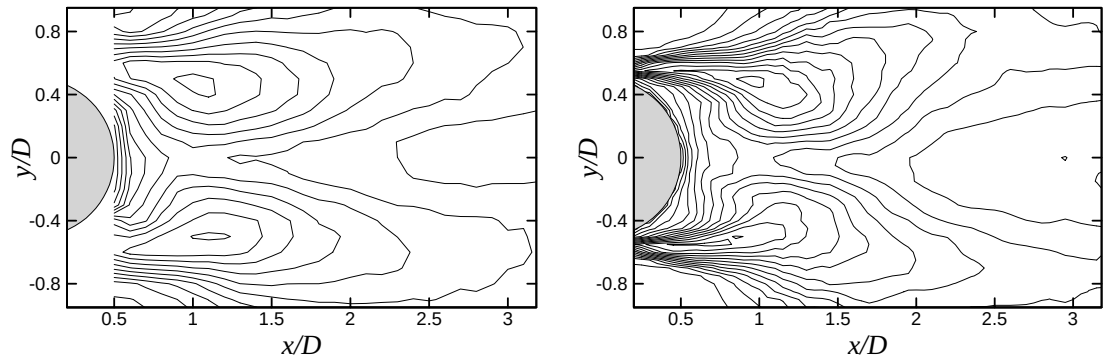

(b)

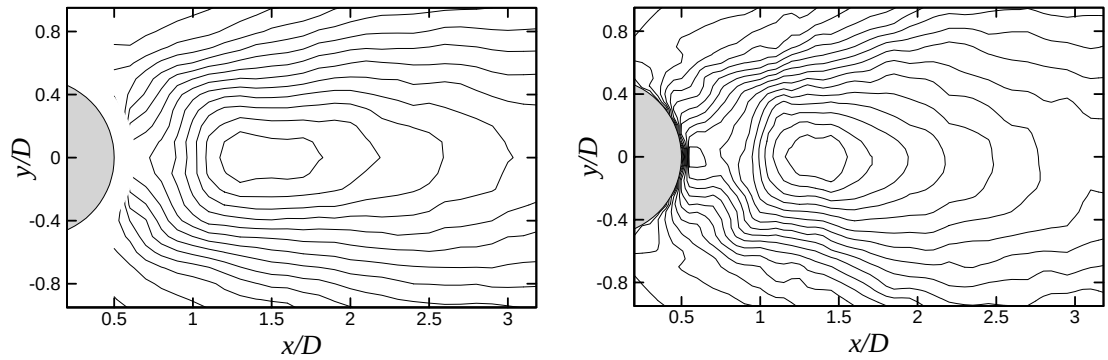

(c)

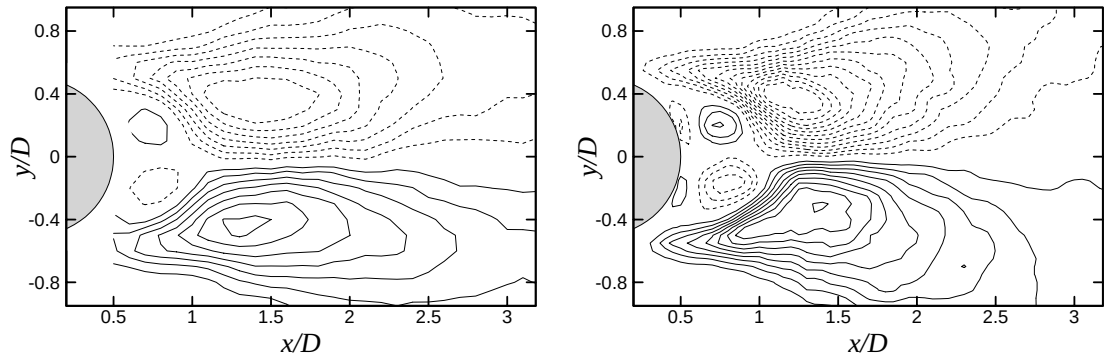

(d)

Figure 1. For caption see next page.

Figure 1. Comparison of flow statistics between experiment (left column; Re = 2150, f_e/f_o = 1.87, $\Delta U/U_m$ = 0.045) and simulation (right column; Re = 2580, f_e/f_o = 1.88, $\Delta U/U_m$ = 0.05); (a) streamwise mean velocity, contours levels: $\overline{u}/U = -0.1, 0, \ldots$; (b) streamwise r.m.s. velocity, contour levels: $u'/U_m = 0.05, 0.1, \ldots$; (c) cross-stream r.m.s. velocity, contour levels: $v'/U_m = 0.05, 0.1, \ldots$; (d) Reynolds shear stress, contour levels $\overline{uv}/U_m^2 = \pm 0.02, \pm 0.04, \ldots$

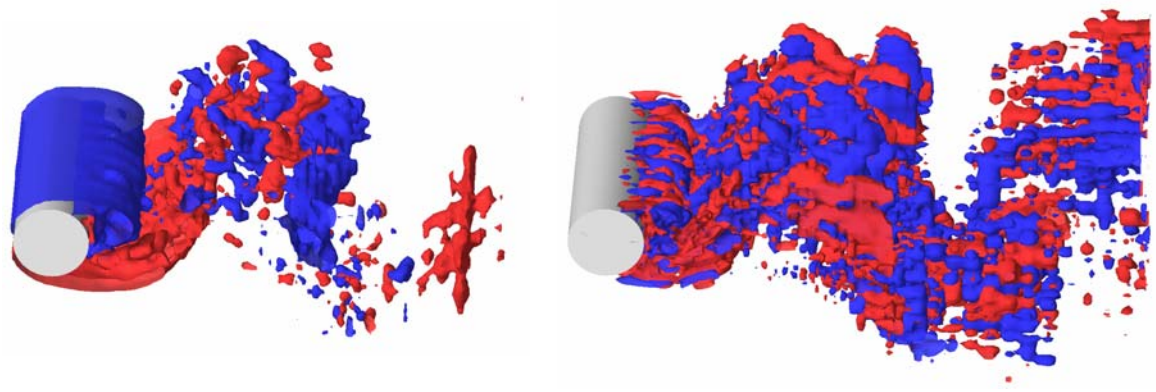

(a) (b)

Figure 2. Three-dimensional view of the instantaneous vorticity distribution in the wake. (a) Isosurfaces of the instantaneous spanwise vorticity; the blue surfaces are for $\omega_z D/U_m = -3$ and the red surfaces for $\omega_z D/U_m = 3$. (b) Isosurfaces of the instantaneous streamwise vorticity; The blue surfaces are for $\omega_x D/U_m = -1$ and the red surfaces for $\omega_x D/U_m = 1$. From the numerical simulation; Re = 2580, f_e/f_o = 1.88, $\Delta U/U_m$ = 0.05.

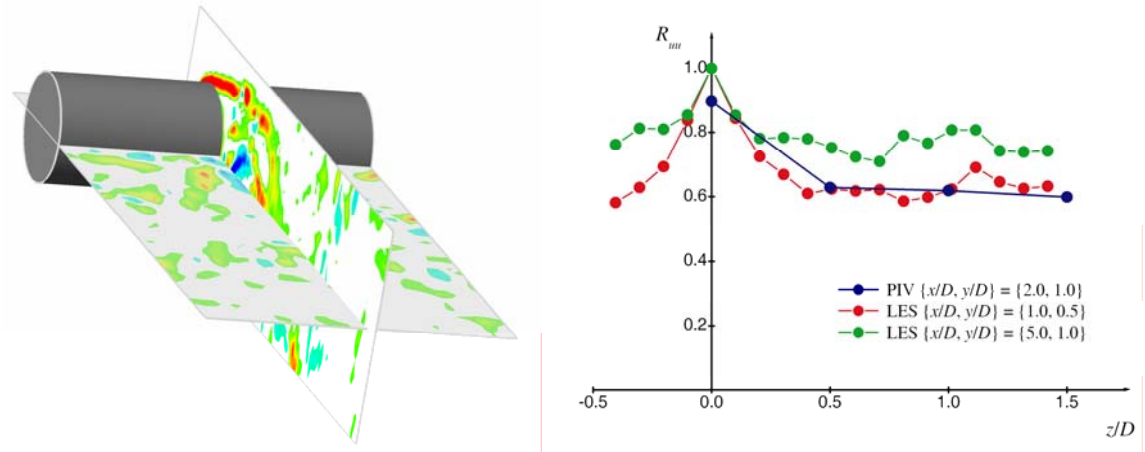

(a) (b)

Figure 3. (a) Three-dimensional view of the instantaneous vorticity distribution in the wake from the simulation. The vorticity components normal to each plane are shown using the same contour levels. (b) Comparison of the spanwise correlation of velocity fluctuations in the separating shear layer from both the experiment and simulation.

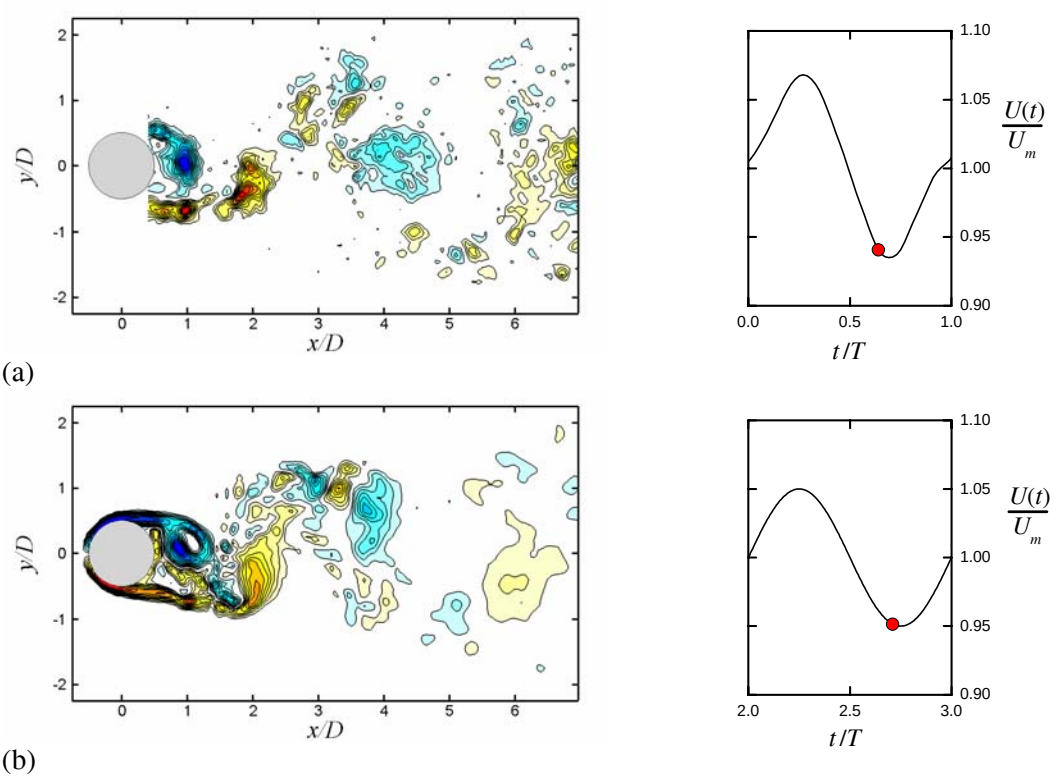

Figure 4. Contours of the instantaneous spanwise vorticity from (a) the experiment (Re = 2165, $f_e/f_o = 1.74$, $\Delta U/U_m = 0.062$) and (b) simulation (Re = 2580, $f_e/f_o = 1.88$, $\Delta U/U_m = 0.05$); the plots on the right side show the corresponding instants during the inflow oscillation; contour levels are the same in both cases, $\omega_z D/U_m = \pm 1, \pm 2 \ldots$

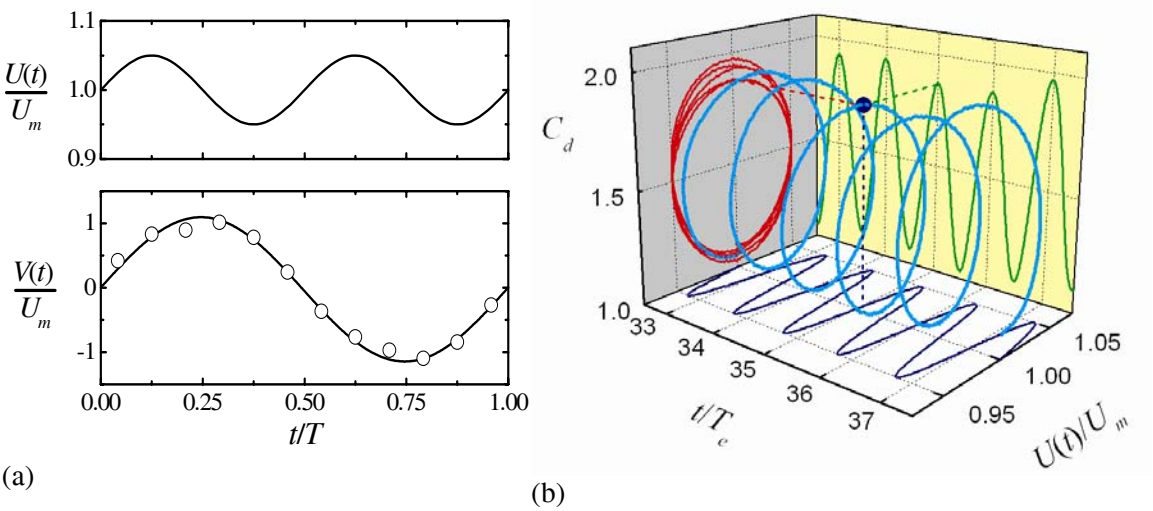

Figure 5. (a) Inflow and flow oscillation across the wake axis at the location of maximum intensity, $x/D = 1.45$; symbols indicate phase-averaged data. (b) Three-dimensional trajectory of the drag coefficient as a function of time and inflow velocity. From the numerical simulation; Re = 2580, $f_e/f_o = 1.88$, $\Delta U/U_m = 0.05$.